

## Evidence for Hydrodynamic Evolution in Proton-Proton Scattering at LHC Energies

K. Werner<sup>(a)</sup>, Iu. Karpenko<sup>(a,b)</sup>, T. Pierog<sup>(c)</sup>, M. Bleicher<sup>(d)</sup>, K. Mikhailov<sup>(e)</sup>

<sup>(a)</sup> *SUBATECH, University of Nantes – IN2P3/CNRS– EMN, Nantes, France*

<sup>(b)</sup> *Bogolyubov Institute for Theoretical Physics, Kiev 143, 03680, Ukraine*

<sup>(c)</sup> *Forschungszentrum Karlsruhe, Institut fuer Kernphysik, Karlsruhe, Germany*

<sup>(d)</sup> *Frankfurt Institute for Advanced Studies (FIAS),*

*Johann Wolfgang Goethe Universitaet, Frankfurt am Main, Germany and*

<sup>(e)</sup> *Institute for Theoretical and Experimental Physics, Moscow, 117218, Russia*

In  $pp$  scattering at LHC energies, large numbers of elementary scatterings will contribute significantly, and the corresponding high multiplicity events will be of particular interest. Elementary scatterings are parton ladders, identified with color flux-tubes. In high multiplicity events, many of these flux tubes are produced in the same space region, creating high energy densities. We argue that there are good reasons to employ the successful procedure used for heavy ion collisions: matter is assumed to thermalizes quickly, such that the energy from the flux-tubes can be taken as initial condition for a hydrodynamic expansion. This scenario gets spectacular support from very recent results on Bose-Einstein correlations in  $pp$  scattering at 900 GeV at LHC.

### I. INTRODUCTION

After one decade of RHIC experiments it seems to be certain that heavy ion collisions at RHIC energies produce a new state of matter which expands as an almost ideal fluid [1–8], whereas proton-proton scattering is usually considered to be a reference system, theoretically well under control via perturbative techniques. Although at very high energy, hadrons experience multiple scatterings when they hit protons or neutrons, inclusive cross sections calculations becomes quite simple due to the fact that different multiple scattering contributions cancel due to destructive interference (AGK cancellations). The corresponding formulas are simple and can be expressed in terms of parton distributions functions, based on evolution equations.

However, in particular at LHC energies where we expect large numbers of scatterings to contribute significantly, it becomes interesting to study event classes corresponding to a large number of scatterings (in practice: high multiplicity events). Here, one needs partial cross sections, corresponding to a particular multiple scattering type (single, or double, or triple...). Gribov-Regge theory provides a solution, in particular when energy sharing is properly taken into account, as in the EPOS approach.

High multiplicity events are very interesting for the following reasons: in EPOS for example, a single scattering amounts to the exchange of a complete parton ladder, including initial state radiation. The whole object is identified as a pair of color flux tubes, which finally break into many pieces (hadrons). In high multiplicity events, with many scatterings involved, we have many partons ladders participating, and therefore a large number of flux tubes sitting essentially on top of each other – as in heavy ion scattering at RHIC. In the heavy ion case, we simply compute the energy density corresponding to these flux tubes (from string theory), assume thermalization, and

then perform a hydrodynamic expansion based on these initial conditions [8].

Since the energy densities reached in high multiplicity proton-proton collisions are comparable to the ones achieved in gold-gold scattering at RHIC, we will apply the same procedure. The usual argument against this approach is the small size of the  $pp$  system, but since we know by now that the size of the space fluctuations in an even-by-event treatment in AuAu scattering is of the order of 1-2 fm, and AuAu seems to be driven by hydrodynamic flow, there is no reason not to do so for high multiplicity  $pp$ .

In this paper, we will briefly review the flux-tube/hydro approach of [8], with special emphasis on  $pp$  scattering. After some elementary checks concerning particle distributions, we come to the main result of this paper: the hydrodynamic expansion modifies drastically the space-time behavior of the evolution, compared to basic picture where the flux-tubes decay independently. And this space-time structure can be clearly “seen” when investigating Bose-Einstein correlations, and the recently published results from ALICE confirm the “hydrodynamic scenario”.

### II. MULTIPLE SCATTERING

#### A. Parton evolution

An elementary scattering within the EPOS approach [8] is given by a so-called “parton ladder”, see fig. 1, representing parton evolutions from the projectile and the target side towards the center (small  $x$ ). The evolution is governed by an evolution equation, in the simplest case according to DGLAP. In the following we will refer to these partons as “ladder partons”, to be distinguished from “spectator partons”. Such a parton ladder

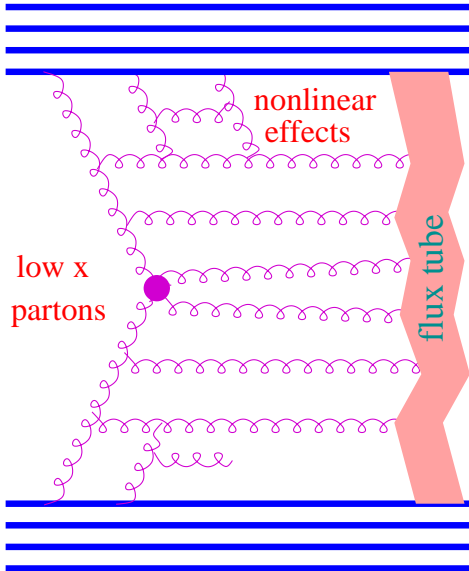


Figure 1: (Color online) Elementary interaction in the EPOS model.

may be considered as a longitudinal color field or flux-tube, conveniently treated as a relativistic string. The intermediate gluons are treated as kink singularities in the language of relativistic strings. This flux tube approach is just a continuation of 30 years of very successful applications of the string picture to particle production in collisions of high energy particles [9–12], in particular in connection with the parton model. An important issue at high energies is the appearance of so-called nonlinear effects, which means that the simple linear parton evolution is no longer valid, gluon ladders may fuse or split. More recently, a classical treatment has been proposed, called Color Glass Condensate (CGC), having the advantage that the framework can be derived from first principles [13–17]. Comparing a conventional string model like EPOS and the CGC picture: they describe the same physics, although the technical implementation is of course different. All realistic string model implementations have nowadays to deal with screening and saturation, and EPOS is not an exception, see [8, 18]. Without screening, proton-proton cross sections and multiplicities will explode at high energies.

A phenomenological treatment of non-linear effects in EPOS employs two contributions: a simple elastic rescattering of a ladder parton on a projectile or target nucleon (elastic ladder splitting), or an inelastic rescattering (inelastic ladder splitting), see fig. 2. The elastic process provides screening, therefore a reduction of total and inelastic cross sections. The importance of this effect should first increase with mass number (in case of nuclei be-

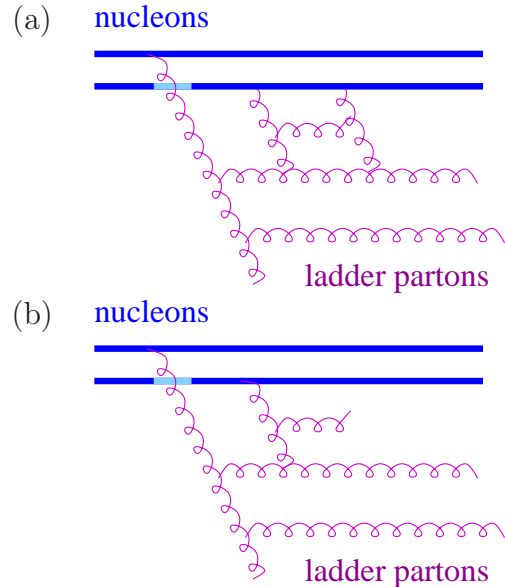


Figure 2: (Color online) (a) Elastic “rescattering” of a ladder parton. We refer to elastic parton ladder splitting; (b) Inelastic “rescattering” of a ladder parton. We refer to inelastic parton ladder splitting.

ing involved), but finally saturate. The inelastic process will affect particle production. Both, elastic and inelastic rescattering must be taken into account in order to obtain a realistic picture.

To include the effects of elastic rescattering, we first parametrize a parton ladder (to be more precise: the imaginary part of the corresponding amplitude in impact parameter space) computed on the basis of DGLAP. We obtain an excellent fit of the form  $\alpha(x^+x^-)^\beta$ , where  $x^+$  and  $x^-$  are the momentum fractions of the “first” ladder partons on respectively projectile and target side (which initiate the parton evolutions). The parameters  $\alpha$  and  $\beta$  depend on the cms energy  $\sqrt{s}$  of the hadron-hadron collision. To mimic the reduction of the increase of the expressions  $\alpha(x^+x^-)^\beta$  with energy, we simply replace them by

$$\alpha(x^+)^\beta + \varepsilon_P (x^-)^{\beta + \varepsilon_T}, \quad (1)$$

where the values of the positive numbers  $\varepsilon_{P/T}$  will increase with the nuclear mass number and  $\log s$ .

The inelastic rescatterings (ladder splittings, looking from inside to outside) amount to providing several ladders close to the projectile (or target) side, which are close to each other in space. They cannot be considered as independent color fields (strings), we should rather think of a common color field built from several partons ladders. We treat this object via an enhancement of remnant excitations. In fact, the picture described so far is not yet complete, since we just considered two interacting partons, one from the projectile and one from the

target. Also the remnants themselves contribute to particle production, but mainly in the fragmentation region. For more details see [8].

### B. Factorization and Multiple Scattering

An inclusive cross section is one of the simplest quantities to characterize particle production. As discussed earlier, inclusive cross section are particularly simple, quantum interference helps to provide simple formulas referred to a “factorization”. If we want to study high multiplicity events, we have to go beyond the inclusive treatment.

To formulate a consistent multiple scattering theory is difficult. A possible solution is Gribov’s Pomeron calculus, which can be adapted to our language by identifying Pomeron and parton ladder. Multiple scattering means that one has contributions with several parton ladders in parallel. This formulation is equivalent to using the eikonal formula to obtain the total cross section from the knowledge of the inclusive one.

We indicated several years ago inconsistencies in this approach, proposing an “energy conserving multiple scattering treatment” [11]. The main idea is simple: in case of multiple scattering, when it comes to calculating partial cross sections for double, triple ... scattering, one has to explicitly care about the fact that the total energy has to be shared among the individual elementary interactions. In other words, the partons ladders which happen to be parallel to each other share the collision energy, see fig. 3. A consistent quantum mechanical formulation of these ideas requires not only the consideration of the usual (open) parton ladders, discussed so far, but also of

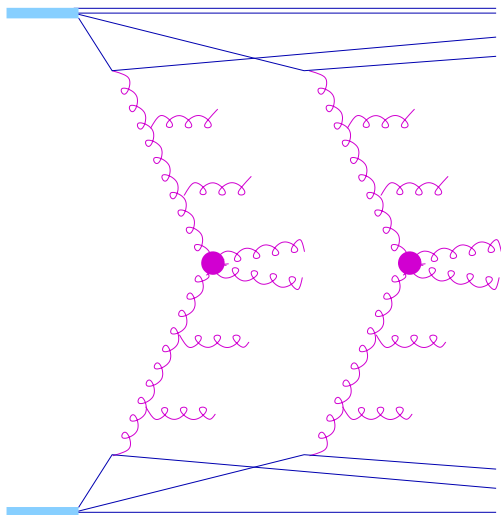


Figure 3: (Color online) Multiple scattering with energy sharing.

closed ladders, representing elastic scattering. These are the same closed ladders which we introduced earlier in connection with elastic rescatterings. The closed ladders do not contribute to particle production, but they are crucial since they affect substantially the calculations of partial cross sections. Actually, the closed ladders simply lead to large numbers of interfering contributions for the same final state, all of which have to be summed up to obtain the corresponding partial cross sections. It is a unique feature of our approach to consider explicitly energy-momentum sharing at this level (the “E” in the name EPOS). For more details see [11].

## III. HYDRODYNAMIC EVOLUTION

### A. Parton-Ladders, Flux-Tubes, Energy-Momentum Tensor

In case of high multiplicity  $pp$  scattering, we apply exactly the same procedure as we did for AuAu collisions at RHIC, as explained in detail in [8], and shortly reviewed in the following. We will identify parton ladders with elementary flux tubes, the latter ones treated as classical strings. We use the simplest possible string: a two-dimensional surfaces  $X(\alpha, \beta)$  in 3+1 dimensional space-time, with piecewise constant initial conditions, referred to as kinky strings. In fig. 4(a), we sketch the space components of this object: the string in  $\mathbb{R}^3$  space is a mainly longitudinal object (here parallel to the  $z$ -axis) but due to the kinks (associated to transversely moving gluons) there are string pieces moving transversely (in  $y$ -direction in the picture). But despite these kinks, most of the string carries only little transverse momentum!

In case of elementary reactions like electron-positron annihilation or proton proton scattering (at moderately relativistic energies), hadron production is realized via string breaking, such that string fragments are identified with hadrons. When it comes to heavy ion collisions or very high energy proton-proton scattering, the procedure has to be modified, since the density of strings will be so high that they cannot possibly decay independently. For technical reasons, we split each string into a sequence of string segments, at a given proper-time  $\tau_0$ , corresponding to widths  $\delta\alpha$  and  $\delta\beta$  in the string parameter space (see fig. 4(b)). One distinguishes between string segments in dense areas (more than some critical density  $\rho_0$  of segments per unit volume), from those in low density areas. The high density areas are referred to as core, the low density areas as corona [21]. String segments with large transverse momentum (close to a kink) are excluded from the core. Based on the four-momenta of infinitesimal string segments,

$$\delta p = \left\{ \frac{\partial X(\alpha, \beta)}{\partial \beta} \delta\alpha + \frac{\partial X(\alpha, \beta)}{\partial \alpha} \delta\beta \right\}, \quad (2)$$

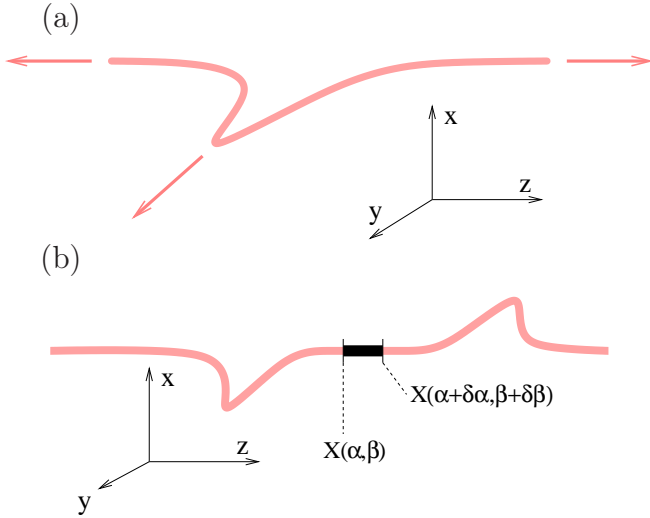


Figure 4: (Color online) (a) Flux tube with transverse kink in  $\mathbb{R}^3$  space. The kink leads to transversely moving string regions (transverse arrow). (b) String segment at given proper time.

with  $g$  being a Gaussian smoothing kernel, one computes the energy-momentum tensor and conserved currents. The corresponding energy density  $\varepsilon(\tau_0, \vec{x})$  and the flow velocity  $\vec{v}(\tau_0, \vec{x})$  serve as initial conditions for the subsequent hydrodynamic evolutions.

In fig. 5, we show as an example the energy density at  $\tau_0 = 0.6 \text{ fm}/c$  for a high multiplicity  $pp$  collision at 900 GeV, where high multiplicity here refers to a plateau

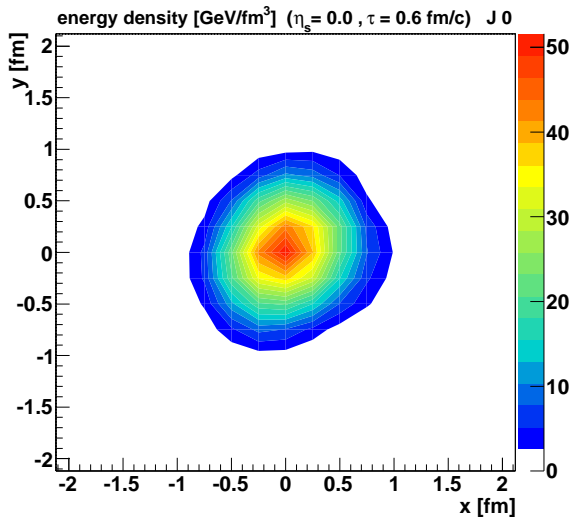


Figure 5: (Color online) Initial energy density in a high multiplicity  $pp$  collision ( $dn/d\eta = 12.9$ ) at 900 GeV, at a space-time rapidity  $\eta_s = 0$ .

height  $dn/d\eta$  of 12.9, which is more than 3 times the average. We see a maximum energy density of about  $50 \text{ GeV}/\text{fm}^3$ , which indeed correspond to the energy densities observed in central gold-gold collisions at 200 GeV. Even more, comparing with the spiky single event results for gold-gold in [8], our  $pp$  distribution correspond to one (of many) spikes in gold-gold at 200 GeV, which means a hydrodynamic treatment for  $pp$  is as good (or bad) as for gold-gold at 200 GeV.

## B. Collective expansion

Having fixed the initial conditions, matter evolves according to the equations of ideal hydrodynamics, namely the local energy-momentum conservation

$$\partial_\mu T^{\mu\nu} = 0, \quad T^{\mu\nu} = (\varepsilon + p) u^\mu u^\nu - p g^{\mu\nu}, \quad (3)$$

and the conservation of net charges,

$$\partial_\mu N_k^\mu = 0, \quad N_k^\mu = n_k u^\mu, \quad (4)$$

with  $k = B, S, Q$ , where  $B$ ,  $S$ , and  $Q$  refer to respectively baryon number, strangeness, and electric charge, and with  $u$  being the four-velocity of the local rest frame. Solving the equations, as discussed in the appendix of [8], provides the evolution of the space-time dependence of the macroscopic quantities energy density  $\varepsilon(x)$ , collective flow velocity  $\vec{v}(x)$ , and the net flavor densities  $n_k(x)$ . Here, the crucial ingredient is the equation of state, which closes the set of equations by providing the  $\varepsilon$ -dependence

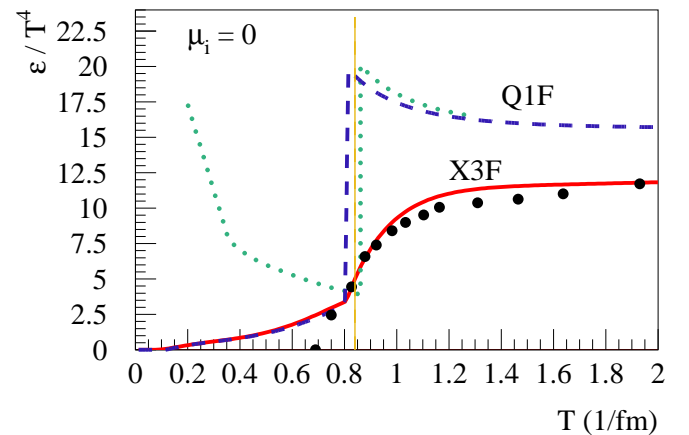


Figure 6: (Color online) Energy density versus temperature, for our equation-of-state X3F (full line), compared to lattice data [22] (points), and some other EoS choices, see [8]. The thin vertical line indicates the “hadronization temperature”  $T_H$ , i.e. end of the thermal phase, when “matter” is transformed into hadrons.

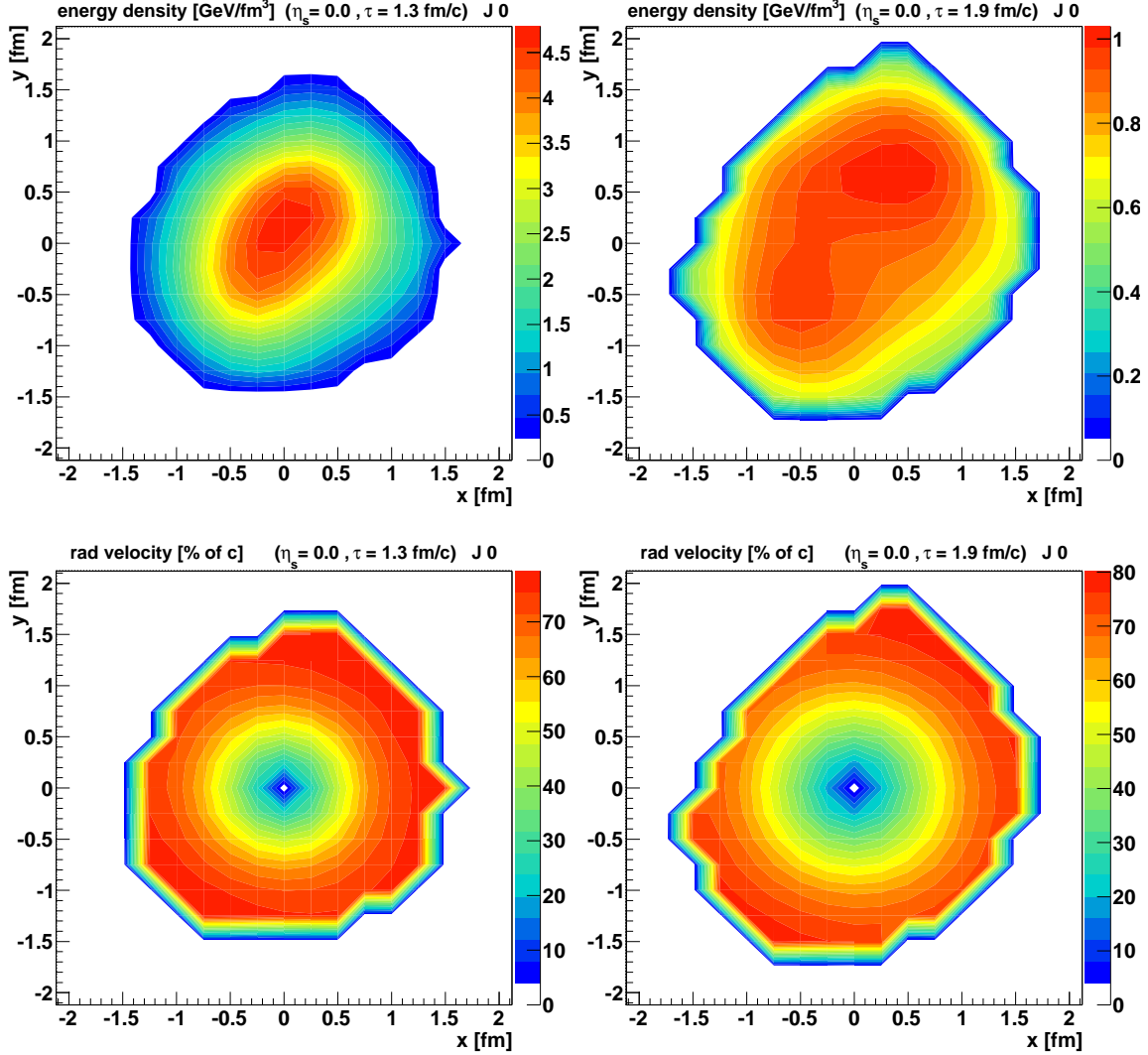


Figure 7: (Color online) Energy density (upper panel) and radial flow velocity (lower panel) for a high multiplicity  $pp$  collision ( $dn/d\eta = 12.9$ ) at 900 GeV, at proper times  $\tau = 1.3$  fm/c (left) and  $\tau = 1.9$  fm/c (right), at a space-time rapidity  $\eta_s = 0$ .

of the pressure  $p$ . As discussed in [8], we use an equation of state compatible with lattice gauge simulations, see fig. 6.

Starting from the flux-tube initial condition, the system expands very rapidly. It hadronizes in the cross-over region, where here “hadronization” is meant to be the end of the completely thermal phase: matter is transformed into hadrons. We stop the hydrodynamical evolution at this point, but particles are not yet free. Our favorite hadronization temperature is 166 MeV, shown as the thin vertical line in fig. 6, which is indeed right in the transition region, where the energy density varies strongly with temperature. At this point we employ statistical hadronization, which should be understood as hadronization of the quark-gluon plasma state into a hadronic sys-

tem, at an early stage, not the decay of a resonance gas in equilibrium.

After this hadronization –although no longer thermal– the system still interacts via hadronic scatterings. The particles at their hadronization positions (on the corresponding hypersurface) are fed into the hadronic cascade model UrQMD [23, 24], performing hadronic interactions until the system is so dilute that no interactions occur any more. The “final” freeze out position of the particles is the last interaction point of the cascade process, or the hydro hadronization position, if no hadronic interactions occurs.

In fig. 7, we show the hydrodynamic evolution of the event corresponding to the initial energy density of fig. 5, which can be considered as a typical example, with simi-

lar observations being true for randomly chosen events of this multiplicity ( $dn/d\eta = 12.9$ ). We see that the system evolves immediately also transversely, the energy density drops very quickly. A very large transverse flow develops, typically around 70 % of the velocity of light. This will have measurable consequences.

#### IV. ELEMENTARY DISTRIBUTIONS

We first check some elementary distributions. We use the EPOS 2.05 version, which has been optimized for heavy ion scattering at RHIC, the same one as used in [8]. We could certainly improve the results by doing some “tuning” taking into account the new LHC results, but the purpose of this paper is more to show what we get from a straight application of the “heavy ion model”, here applied to  $pp$  at LHC. We only consider 900 GeV, for higher energies some reconsideration of our screening procedures will be necessary (work in progress). As usual we work with the event-by-event mode, and hydrodynamics is only employed for high density areas (core-corona separation).

In the following we will compare three different scenarios:

**full** : the full calculations, including hydro evolution and hadronic cascade;

**no casc** : calculation without hadronic cascade;

**base** ; calculation without hydro and without cascade.

We will compare the corresponding calculations with experimental data, for  $pp$  scattering at 900 GeV.

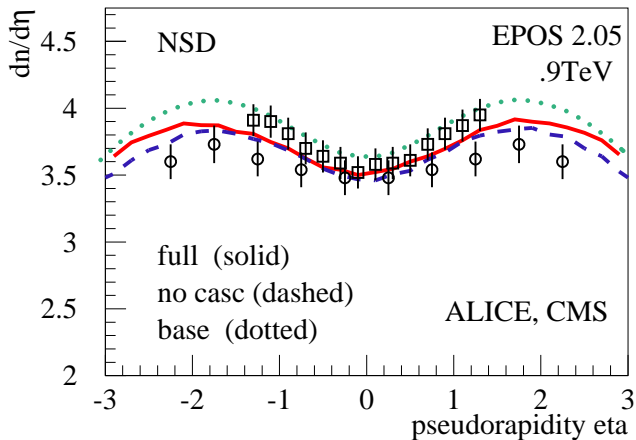


Figure 8: (Color online) Pseudorapidity distributions in  $pp$  scattering at 900 GeV, compared to data (points). We show the full calculation (solid line), a calculation without hadronic cascade (dashed), and a calculation without hydro and without cascade (dotted).

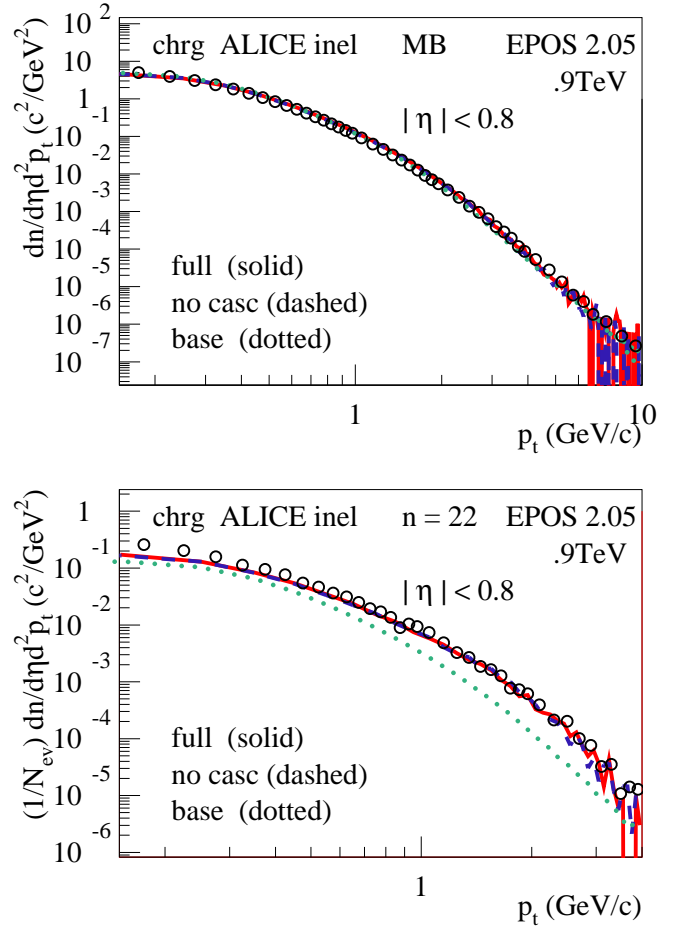


Figure 9: (Color online) Transverse momentum distributions in  $pp$  scattering at 900 GeV, for minimum bias events (upper panel) and high multiplicity events ( $n = 22$ , lower panel), compared to data (points). We show the full calculations (solid lines), a calculation without hadronic cascade (dashed), and a calculation without hydro and without cascade (dotted).

In fig. 8, we show pseudorapidity distributions of charged particles, compared to data from CMS [25] and ALICE [26, 27]. The three scenarios do not differ very much, and agree roughly with the data.

We then investigate transverse momentum distributions. For minimum bias events, there is again little difference for the three scenarios (all of them reproduce the data within 20%), as seen in the upper panel of fig. 9. The situation changes drastically, when we consider high multiplicity events, see the lower panel of fig. 9. Here the base calculation (without hydro) underestimates the data by a factor of three, whereas the full calculation gets close to the data. This is a very typical behavior of collective flow: the distributions get harder at intermediate values of  $p_t$  (around 1-4 GeV/c).

In fig. 10, we plot the mean transverse momentum as

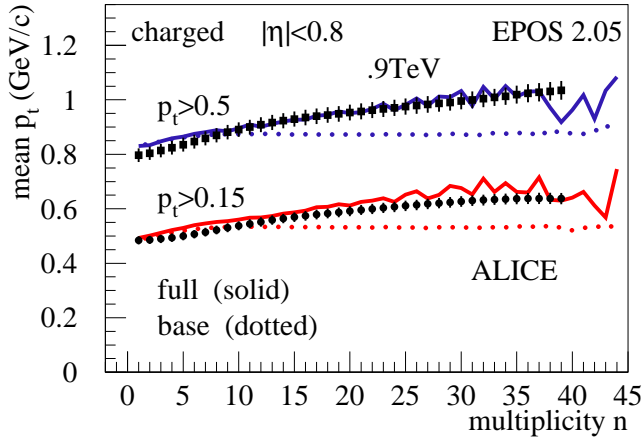


Figure 10: (Color online) Mean transverse momentum as a function of the charged multiplicity in  $pp$  scattering at 900 GeV, compared to data (points). We show the full calculation (solid line), and a calculation without hydro and without cascade (dotted).

a function of the charged multiplicity, compared to data from ALICE [27]. The increase of the mean  $p_t$  with multiplicity is in our approach related to collective flow: with increasing multiplicity one gets higher initial energy densities, and more collective flow can develop. The data are therefore compatible with our flow picture, but for a real proof one needs at least in addition the mean  $p_t$  behavior of heavier particles (protons, lambdas, or even heavier), since the effect gets bigger with increasing mass.

## V. BOSE-EINSTEIN CORRELATIONS

The space-time evolution of the “full” hydrodynamic approach will be completely different compared to the “base” approach, where particles are directly produced from breaking strings, as can be seen from fig. 11, where we plot the distribution of formation points of  $\pi^+$  as a function of the radial distance

$$r = \sqrt{x^2 + y^2} \quad (5)$$

(in the  $pp$  center of mass system (cms)). Only particles with space-time rapidities around zero are considered. We compare again the three scenarios “full” (full calculation - flux-tube initial conditions, hydro, hadronic cascade), “no casc” (without hadronic cascade, only flux-tube initial conditions and hydro, hadronization as usual at 166 MeV), and “base” (without hydro and without cascade, just flux-tube approach with string decay).

All calculations in this section refer to high multiplicity events in  $pp$  scattering at 900 GeV, with a mean  $dn/d\eta(0)$  equal to 12.9. The “base calculation” (dotted line) gives

as expected a steeply falling distribution as a function of  $r$ . In the two cases involving a hydrodynamical evolution, particle production is significantly delayed, even more in the case of the full calculation, with hadronic cascade. The bump in the two latter scenarios is due to particles being produced from the fluid, the small  $p_t$  contribution is due to corona particles.

This particular space-time behavior of the hydrodynamic expansions should clearly affect Bose-Einstein correlations – what we are going to investigate in the following. There is a long history of so-called femtoscopic methods [28–32], where the study of two-particle correlations provides information about the source function  $S(\mathbf{P}, \mathbf{r}')$ , being the probability of emitting a pair with total momentum  $\mathbf{P}$  and relative distance  $\mathbf{r}'$ . Under certain assumptions, the source function is related to the measurable two-particle correlation function  $CF(\mathbf{P}, \mathbf{q})$  as

$$CF(\mathbf{P}, \mathbf{q}) = \int d^3r' S(\mathbf{P}, \mathbf{r}') |\Psi(\mathbf{q}', \mathbf{r}')|^2, \quad (6)$$

with  $\mathbf{q}$  being the relative momentum, and where  $\Psi$  is the outgoing two-particle wave function, with  $\mathbf{q}'$  and  $\mathbf{r}'$  being relative momentum and distance in the pair center-of-mass system. The source function  $S$  can be obtained from our simulations, concerning the pair wave function, we follow [33], some details are given in [8].

Here, we investigate  $\pi^+ - \pi^+$  correlations. We evaluate eq. (6), with Bose-Einstein (BE) quantum statistics included, but no Coulomb corrections. Weak decays are not carried out. In figs. 12, 13, 14, we show the results for different  $k_T$  intervals defined as (in MeV):  $KT1 = [100, 250]$ ,

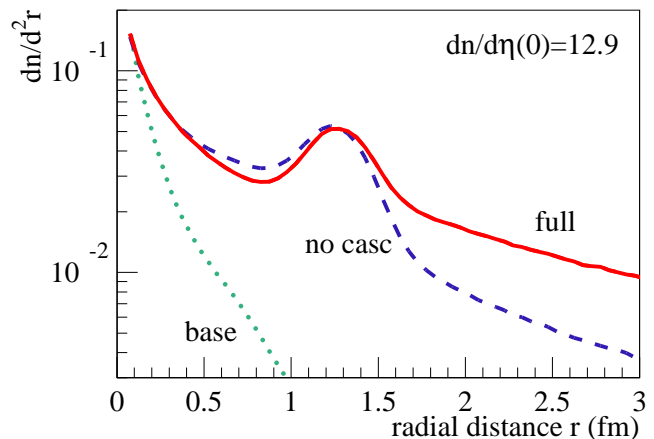


Figure 11: (Color online) The distribution of formation points of  $\pi^+$  as a function of the radial distance in a high multiplicity event from  $pp$  scattering at 900 GeV, for the following scenarios: the full calculation (solid line), a calculation without hadronic cascade (dashed), and a calculation without hydro and without cascade (dotted).

KT3= [400, 550], KT5= [700, 1000], where  $k_T$  of the pair is defined as

$$k_T = \frac{1}{2} (|\vec{p}_t(\text{pion 1}) + \vec{p}_t(\text{pion 2})|). \quad (7)$$

We compare the three different scenarios: “full calculation” (solid line), “calculation without hadronic cascade” (dashed), and “calculation without hydro and without cascade” (dotted), and data from ALICE [34]. The data are actually not Coulomb corrected, because the effect is estimated to be small compared to the statistical errors. We consider here the high multiplicity class, with  $dn/d\eta(0) = 11.2$ , close to the value of 12.9 from our simulated high multiplicity events. We compare with the real data (not polluted with simulations), normalized via mixed events, and we do the same with our simulations. Despite the limited statistics, in particular at large  $k_T$ , we see very clearly that the “full” scenario, including hydro evolution and hadronic cascade, seems to fit the data much better than the two other ones. Usually people like to extract radii from these distributions, so when we make a fit of the form

$$CF - 1 = \lambda \exp(-R|\mathbf{q}|), \quad (8)$$

in the  $|\mathbf{q}|$  range from 0.05 to 0.70. We obtain the radii given in the figure. So the radii are very different, varying from 0.69 fm (base approach) to 1.80 fm (full model), which is understandable from fig. 11. We prefer an exponential fit rather than a Gaussian, simply because the former one works, the latter one does not. We do not want to give a precise meaning to  $R$ , it simply characterizes the distribution.

Normalizing by mixed events is something one can easily do experimentally (this is why we compare with these

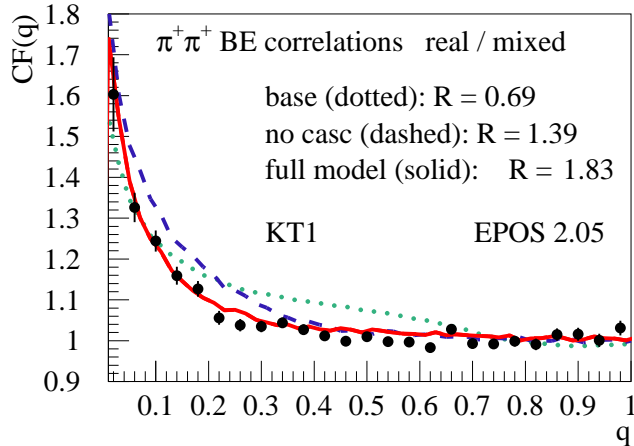


Figure 12: (Color online) The correlation functions  $CF$  for  $\pi^+ \pi^+$  pairs as obtained from our simulations, for the three different scenarios, for  $k_T$  bin KT1, compared to data (points).

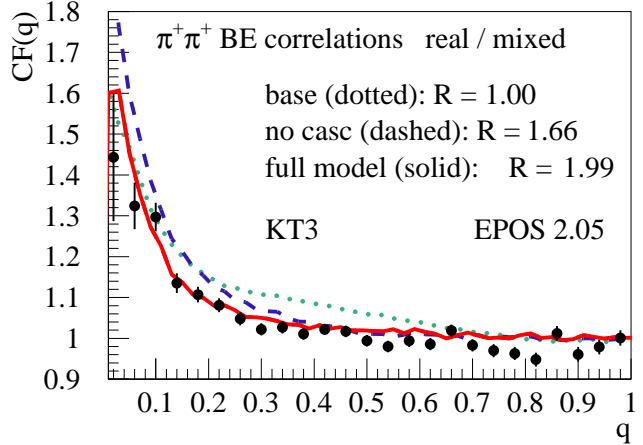


Figure 13: (Color online) Same as fig. 12, but  $k_T$  range KT3.

data), but it is clear that one has still unwanted correlations, like those due to energy-momentum conservation, which is not an issue in mixed events. Doing simulations, life is easier. We can take simulations without Bose-Einstein correlations as base line, rather than mixed events. This is referred to as “real / bare” normalization (to be distinguished from the “real / mixed” case discussed earlier). The corresponding results are shown in fig. 15, the solid line (full calculation) is now completely horizontal away from the peak region, the radius from the exponential fit is 2.10 fm instead of 1.80 fm for the “mixed” normalization. For the other  $k_T$  regions, the situation is similar, the final results for all three  $k_T$  regions for the full calculation is shown in fig. 16, together with the radii from the exponential fit: they are almost identical, around 2 fm.

We get to the same conclusion as outlined in [34]: the

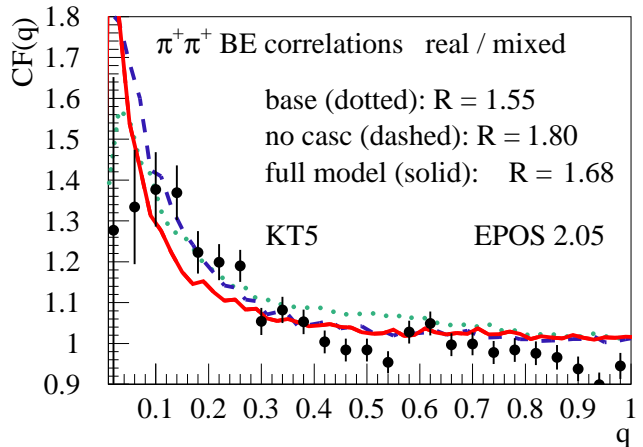


Figure 14: (Color online) Same as fig. 12, but  $k_T$  range KT5.

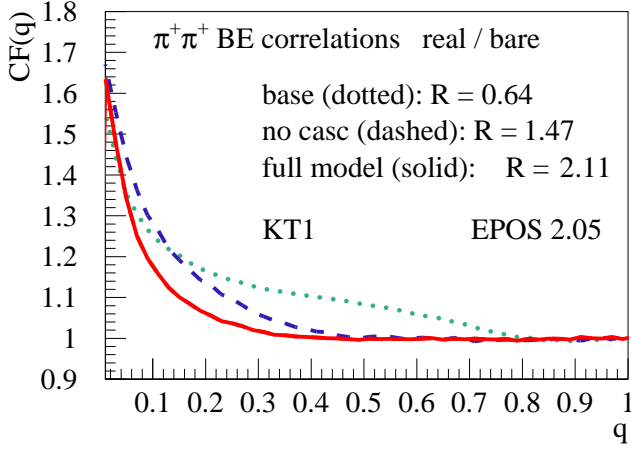


Figure 15: (Color online) Same as fig. 12, but normalization via a simulation w/o BE correlation (“bare”).

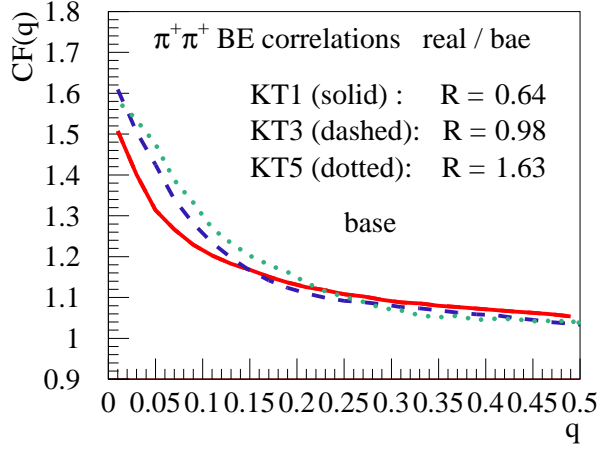


Figure 17: (Color online) As fig. 16, but calculation without hydro and without cascade.

radii are  $k_T$  independent, contrary to what has been observed in AuAu scattering.

How can it be that our hydrodynamic scenario gives a strong  $k_T$  dependence in AuAu, but not in  $pp$ ? To answer this question, we compute the “true” correlation function (real / bare normalization) for the calculation without hydro and without cascade (just string decay). The results are shown in fig. 17. Surprisingly, here we get a strong  $k_T$  dependence of the radii, but the “wrong” way: we have 0.64 for KT1 and 1.63 fm for KT5 ! Actually such a behavior is quite normal, as seen from fig. 18: the distribution is broader for high  $p_t$  particles, because high  $p_t$  resonances live longer and can move further out before decaying. This effect is in principle also present in AuAu scattering, but it is much more visible for the

small  $pp$  system. So in  $pp$  we have two competing effects:

- radii increase with  $k_T$ , due to the bigger size of the source of the high  $p_t$  particles compared to the low  $p_t$  ones,
- radii decrease with  $k_T$ , as in AuAu (see [8]), in case collective flow, due to the  $p-x$  correlation.

As seen in fig. 19, this  $p-x$  correlation exists indeed for the case of hydrodynamic evolutions, and is much smaller in the basic scenario. So in the hydro scenarios, the two competing effects roughly cancel, the radii are  $k_T$  independent. To really see the  $x-p$  correlation, one need to “divide out” the trivial  $k_T$  dependence due to the  $p_t$

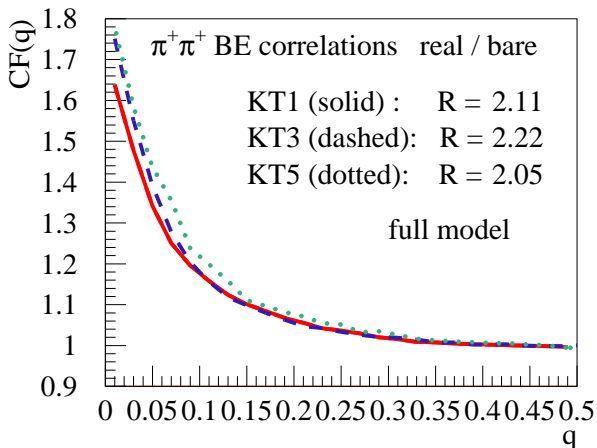


Figure 16: (Color online) Correlation function, normalized by using a simulation w/o BE correlation (“bare”), for three  $k_T$  intervals.

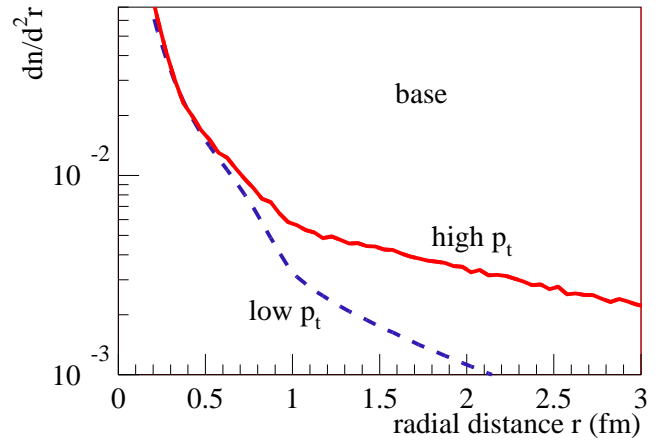


Figure 18: (Color online) The distribution of formation points of particles as a function of the radial distance, for the scenario “without hydro and without cascade”, for high  $p_t$  and low  $p_t$  particles.

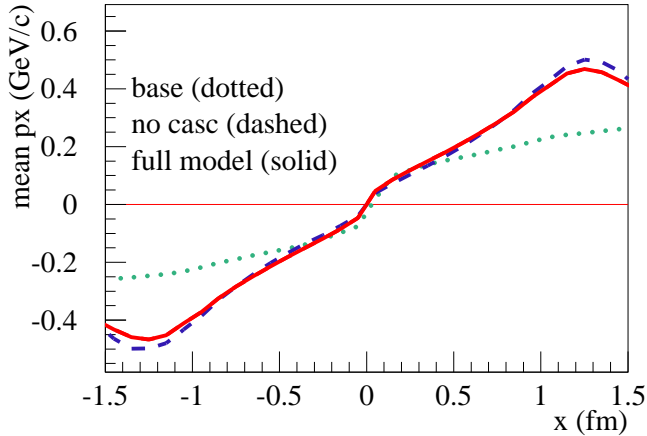


Figure 19: (Color online) Momentum – space correlation, for the different scenarios.

dependence of the single particle source sizes, which we do by considering the  $k_T$  dependence of  $R/R_{\text{bas}}$ , with the reference radius  $R_{\text{bas}}$  referring to the base scenario (without hydro, without cascade), see fig. 20: The ratio  $R/R_{\text{bas}}$  decreases with  $k_T$  as a manifestation of the  $x - p$  correlation, as a consequence of the hydrodynamic expansion.

An alternative way of getting out unwanted correlations would be the consideration of double ratios like

$$\frac{CF(\text{full scenario with BE})/CF(\text{full scenario w/o BE})}{CF(\text{base scenario with BE})/CF(\text{base scenario w/o BE})}, \quad (9)$$

where basic scenario refers to the calculation without hydro and without hadronic cascade.

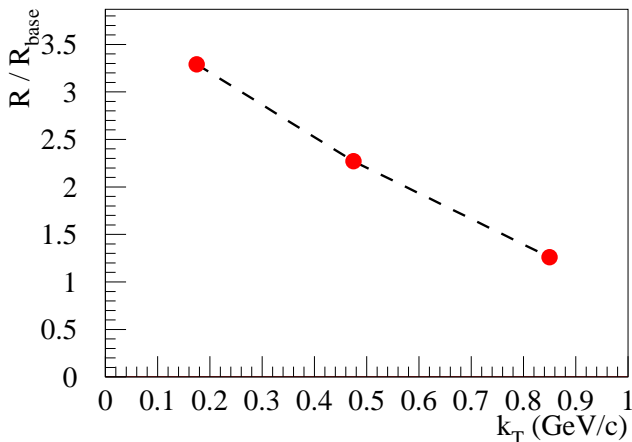


Figure 20: (Color online) The  $k_T$  dependence of  $R/R_{\text{bas}}$ . The ratio decreases significantly with  $k_T$ , a clear “flow signal”.

## VI. SUMMARY

After having introduced recently a sophisticated approach of hydrodynamic expansion based on flux-tube initial conditions for AuAu collisions at RHIC, we now employ exactly the same picture to  $pp$  scattering at 900 GeV, which is in particular justified for high multiplicity events. A very interesting application are Bose-Einstein correlations. We have shown that as in heavy ion scattering the hydrodynamic expansion leads to momentum – space correlations, which clearly affect the correlation functions. To see the signal is non-trivial due to the fact that in addition to the  $x - p$  correlations (which leads to decreasing radii with  $k_T$ , there is a second effect which works the other way round: the single particle source size is  $p_t$  dependent, which is an important effect in  $pp$ , not so in heavy ion scattering. In this sense we can interpret the  $k_T$  independence of the radii as a real flow effect. Our simulation does not only reproduce the  $k_T$  independence, but also the whole correlation functions, which is not at all reproduced from the “base scenario” without hydro and without cascade. So the correlation data provide a very strong evidence for a collective hydrodynamic expansion in  $pp$  scattering at the LHC.

## Acknowledgments

This research has been carried out within the scope of the ERG (GDRE) “Heavy ions at ultra-relativistic energies”, a European Research Group comprising IN2P3/CNRS, Ecole des Mines de Nantes, Université de Nantes, Warsaw University of Technology, JINR Dubna, ITEP Moscow, and Bogolyubov Institute for Theoretical Physics NAS of Ukraine. Iu. K. acknowledges partial support by the MESU of Ukraine, and Fundamental Research State Fund of Ukraine, agreement No F33/461-2009. Iu.K. and K.W. acknowledge partial support by the Ukrainian-French grant “DNIPRO”, an agreement with MESU of Ukraine No M/4-2009. T.P. and K.W. acknowledge partial support by a PICS (CNRS) with KIT (Karlsruhe). K.M. acknowledges partial support by the RFBR-CNRS grants No 08-02-92496-NTsNIL\_a and No 10-02-93111-NTsNIL\_a.

- 
- [1] P. Huovinen, P. F. Kolb, U. W. Heinz, P. V. Ruuskanen and S. A. Voloshin, Phys. Lett. B 503 (2001) 58
- [2] T. Hirano and K. Tsuda, Phys. Rev. C 66 (2002) 054905T.
- [3] S.A.Bass and A.Dumitru, Phys. Rev. C 61, 064909 (2000)
- [4] D. Teaney, J. Lauret and E. V. Shuryak, Phys. Rev. Lett.86, 4783 (2001)
- [5] T. Hirano, U.W.Heinz, D. Kharzeev, R. Lacey and Y. Nara, Phys. Lett. B 636 (2006) 299
- [6] C. Nonaka and S. A. Bass, Nucl. Phys. A 774, 873 (2006); and Phys. Rev. C 75, 014902 (2007)
- [7] R.P.G. Andrade, F. Grassi, Y. Hama, T. Kodama, W.L. Qian, Phys.Rev.Lett.101:112301,2008
- [8] K.Werner, Iu.Karpenko, T.Pierog, M. Bleicher, K. Mikhailov, arXiv:1004.0805, to be published in Phys. Rev. C
- [9] B. Andersson, G. Gustafson, G. Ingelman, and T. Sjostrand, Phys. Rept. 97, 31, 1983
- [10] K. Werner, Phys. Rep. 232, 87, 1993
- [11] H. J. Drescher, M. Hladik, S. Ostapchenko, T. Pierog and K. Werner, Phys. Rept. 350, 93, 2001
- [12] A. Capella, U. Sukhatme, C.-I. Tan, and J. {Tran Thanh Van}, Phys. Rept. 236, 225, 1994
- [13] L.D. McLerran, R. Venugopalan, Phys. Rev. D 49, 2233 (1994). *ibid.* D49, 3352 (1994); D 50, 2225 (1994)
- [14] Yu.V. Kovchegov, Phys. Rev. D 54, 5463 (1996)
- [15] E. Iancu, R. Venugopalan, Quark Gluon Plasma 3, Eds. R.C. Hwa, X.N.Wang, World Scientific, hep-ph/0303204
- [16] A. Kovner, L.D. McLerran, H. Weigert, Phys. Rev. D 52, 3809 (1995); *ibid.*, D 52, 6231 (1995).
- [17] F. Gelis, E. Iancu, J. Jalilian-Marian, R. Venugopalan, arXiv:1002.0333, submitted to the Annual Review of Nuclear and Particle Sciences
- [18] Klaus Werner, Fu-Ming Liu, Tanguy Pierog, Phys. Rev. C 74, 044902 (2006), arXiv: hep-ph/0506232
- [19] M. Bleicher, F. M. Liu, A. Keränen, J. Aichelin, S.A. Bass, F. Becattini, K. Redlich, and K. Werner, Phys.Rev.Lett.88, 202501, 2002.
- [20] F.M. Liu, J.Aichelin, M.Bleicher, H.J. Drescher, S. Ostapchenko, T. Pierog, and K. Werner, Phys. Rev. D67, 034011, 2003
- [21] K. Werner, Phys. Rev. Lett. 98, 152301 (2007)
- [22] Y. Aoki, Z. Fodor, S.D. Katz , K.K. Szabo, JHEP 0601:089, 2006
- [23] M. Bleicher et al., J. Phys. G25 (1999) 1859
- [24] H. Petersen, J. Steinheimer, G. Burau, M. Bleicher and H. Stocker, Phys. Rev. C78 (2008) 044901
- [25] CMS Collaboration, J. High Energy Phys. 02 (2010) 041
- [26] ALICE collaboration, arXiv:1007.0719
- [27] K. Aamodt et al., ALICE collaboration, Eur. Phys. J. C68 (2010) 89-108
- [28] G. I. Kopylov and M. I. Podgoretsky, Sov. J. Nucl. Phys. 15, 219 (1972). [2]
- [29] G. I. Kopylov and M. I. Podgoretsky, Sov. J. Nucl. Phys. 18, 336 (1974).
- [30] S. Pratt, Phys. Rev. Lett. 53:1219-1221,1984
- [31] M. A. Lisa, Scott Pratt , Ron Soltz, Urs Wiedemann, Ann. Rev. Nucl. Part.Sci.55:357-402, 2005, nucl-ex/0505014
- [32] A. Kisiel, W. Florkowski, W. Broniowski, Phys.Rev.C73:064902,2006, nucl-th/0602039
- [33] R. Lednicky, Physics of Particles and Nuclei 40 (2009) 307
- [34] ALICE collaboration, arXiv:1007.0516